First-principles calculations of charged surfaces and interfaces: A plane-wave nonrepeated slab approach

M. Otani and O. Sugino
Institute for Solid State Physics, University of Tokyo, 5-1-5 Kashiwanoha, Kashiwa 277-8581, Japan
and CREST, Japan Science and Technology Agency, 4-1-8 Honcho Kawaguchi, Saitama, Japan
(Received 15 September 2005; revised manuscript received 10 November 2005; published 13 March 2006)

A new first-principles computational approach to a charged surface/interface is presented. The surface is modeled as a slab imposed with boundary conditions to screen the excess surface charge. To treat this model, which is nonperiodic in the surface normal direction, a standard pseudopotential plane-wave scheme is modified at the Poisson solver part with the help of the Green's function technique. Benchmark calculations are done for Al/Si(111) with the bias voltage applied between the surface and the model scanning tunneling microscopy (STM) tip, the model back gate, or the model solution. The calculations are found to be efficient and stable, and their implementation is found to be easy. Because of the flexibility, the scheme is considered to be applicable to more general experimental situations.

DOI: 10.1103/PhysRevB.73.115407 PACS number(s): 73.30.+y, 68.35.Md, 73.20.−r, 31.15.Ew

I. INTRODUCTION

Understanding of electronic and geometric properties of surfaces and interfaces has been greatly advanced by virtue of the increasing number of first-principles calculations based on the density functional theory (DFT).[1,2] A large number of such works make use of the computational scheme based on the plane-wave (PW) basis set, pseudopotential (PP) scheme, and repeated slab geometry.[3] This scheme is very flexible in describing various surface-interface geometries in both the surface and vacuum regions. It is reasonably accurate in describing electronic structures, atomic force, and a stress tensor with a moderate cost of computational time. It is also readily combined with advanced computational methods such as molecular dynamics (MD) simulation. Numerous algorithms have been developed so far; the scheme serves a wide variety of applications.

Since this approach handles all degrees of freedom within the supercell quantum mechanically, however, the cell size is limited to typically a few nanometers, even using modern supercomputers.[4–6] Therefore, modeling is severely restricted for some problems by supercell geometry, or the periodic boundary condition (PBC) imposed on the cell. Typical examples of such problems are the following.

For studying the work function, we require the Fermi level, μ, referred to the vacuum level, for which we need to determine the potential profile between surface and infinity. When an electrode, such as that used in a scanning tunneling microscopy (STM) tip, exists at some distance away from the surface of grounded substrate, μ referred to the electrode potential is the relevant quantity. The value of μ, which is controllable experimentally by changing the bias voltage, strongly affects the potential profile between the surface and electrode. When that region is filled with a solution, the system constitutes a kind of battery, in which a variety of electrochemical processes can occur. These problems are difficult to model when imposing the PBC in the surface normal direction, say the z direction. Use of a basis set other than the PW, such as a real-space mesh or atomic orbitals, might be a way of overcoming those problems, but considering other advantages that are inherent in the DFT-PW-PP scheme, it is very important to extend the scheme, using minimal modification, to thereby allow its application to such problems. In this context, this paper describes such DFT-PW-PP based methods and shows its applicability.

Our approach consists of solving the Poisson equation in the whole region under study, which is, for example, $z \in [-\infty, \infty]$ when handling the slab sandwiched by vacua. This task is accomplished with the help of Green's function technique. The Kohn-Sham equation, on the other hand, is solved in a cell of finite length in the z direction imposing the PBC. Such a treatment is allowed when the electrons are not extended much beyond the surface region, but are instead confined within a certain region near the surface. For that reason, although we use an isolated slab geometry instead of the repeated slab and use a corresponding Poisson solver, we use the Kohn-Sham solver of the repeated slab. Thereby, we restrict our study to a situation in which the surface and the electrode are electronically disconnected.

In this respect, our approach is clearly distinguishable from those that are frequently adopted to study the nonequilibrium electronic current flowing through a molecular device between the source and drain electrodes. In those cases, it is essential to solve the Kohn-Sham equation or the corresponding Green's function imposing the open boundary condition to obtain the electrons in the scattering state.[7–9] In contrast, in our approach, the current is negligibly small in our target systems and the electrons in the ground state are given particular attention.

When electronically disconnected from the electrode, the surface is generally charged up because of the applied bias and is exposed to the electric field that is generated between the surface and electrode. The electric field might be interpreted as being generated from both the surface charge and its image charge in the electrode. This interpretation is justified particularly when the electrode is modeled as a continuum of perfect conductors.

Specifically addressing the surface exposed to the electric field, several precedent works[10,11] have used an external po-

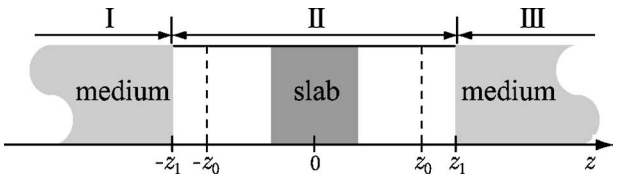

FIG. 1. Schematic drawing of a slab geometry sandwiched by semi-infinite media. z_0 and z_1, respectively, denote the cell boundary for repeated slab calculations and the interface between the vacuum and the medium.

tential that is linear in the slab region and bent near the cell boundary, i.e., the sawlike potential, that adapts to the repeated slab geometry. For the charged surface exposed to the electric field, Ho *et al.*[12] and Fu *et al.*[13] used a repeated slab model in which a planar neutralizing charge sheet is put at the cell boundary. The charge sheet avoids divergence of the electrostatic energy. In this model, the electric field originated from the excess surface charge is generated between the surface and the charge sheet. These works demonstrate that it is possible to compute the surface that is charged up and/or exposed to an electric field within the repeated slab technique. By removing the PBC in the surface normal direction, however, modeling can be accomplished more flexibly. Consequently, modeling would be able to take explicit account of the image charge contribution; we could also put external charges at some distance away, as is often done in cluster model approaches. Introducing such flexibility into a DFT-PW-PP based scheme is the salient motivation of this study.

More specifically, we treat an isolated slab that is sandwiched by semi-infinite media of relative permittivity $\epsilon(\boldsymbol{r})$, with which to describe vacuum, conductor, or solution within a level of a macroscopic continuum model (see Fig. 1). The Poisson equation is then modified as

$$\nabla \cdot [\epsilon(\boldsymbol{r}) \nabla] V(\boldsymbol{r}) = -4\pi \rho_{\mathrm{tot}}(\boldsymbol{r}). \tag{1}$$

When we introduce a region of infinite permittivity, the medium works as a perfect conductor. On the other hand, when the permittivity is finite and has the value of water molecules in the liquid phase (78.4), the surface can be considered as being in contact with water. If the value of ϵ is one, the surface is, of course, exposed to ultrahigh vacuum (UHV). An important advantage of our scheme is that the potential can be obtained in reference to the value at infinity. This enables determination of the Fermi level, below which electrons are accommodated. Therefore, we can perform electronic structure calculations under the constant μ condition, which has been asserted as very important to treat electrode problems.[14]

The total charge density $\rho_{\mathrm{tot}}(\boldsymbol{r})$ in Eq. (1) consists not only of charges of the electrons and nuclei, but also of external charges that are located additionally. As the external charge, we would be able to introduce classical charge density $\rho_{\mathrm{c}}(\boldsymbol{r})$ that would be determined according to the solution theory, such as the Poisson-Boltzmann (PB) theory[15] in which $\rho_{\mathrm{c}}(\boldsymbol{r})$ is determined statistically based on the electrostatic potential $V(\boldsymbol{r})$. It is important to point out that, by introducing $\rho_{\mathrm{c}}(\boldsymbol{r})$ of solution theory, charge neutrality is satisfied automatically in the whole region, Ω, as

$$\int_{\Omega} \rho_{\mathrm{tot}}(\boldsymbol{r}) d\boldsymbol{r} = 0, \tag{2}$$

and the system of weak screening (long screening length) can be described with a modest computational time. This is an advantage over the repeated slab approach in which an extremely large supercell is required.

The remainder of this paper presents details of this scheme, in which four explicit formulations are made for the slab in contact with the vacuum, conductor, and solution. Furthermore, we demonstrate its applicability using the benchmark calculations of the Al/Si(111) surface, i.e., the Si(111) 1×1 surface with an aluminum adlayer. Those calculations confirmed that our scheme reproduces the total energy obtained by the repeated slab calculation in which a comparison is possible; the computational time required for the electronic structure calculation and force calculation are comparable between the two schemes.

The separated treatment of the Poisson equation and the Kohn-Sham equation, which is the essence of our scheme, is considered to have potentialities for providing more flexible modeling of the surface/interface, although the formulation and calculation were done for the four selected cases just for illustration. In particular, for the solution, we used one of the simplest continuum theories, i.e., the PB theory, as a first step. We consider that great improvement might be achieved if our scheme were combined with the multiscale "quantum mechanics and molecular mechanics (QM/MM)" models[16–18] or advanced liquid theory such as the reference interaction site model (RISM-SCF),[19] but the work in that direction is beyond the scope of this paper and is left for future studies.

II. METHOD OF CALCULATION

A. Slab model for the surface and interface

For description of the surface and interface, we use a slab geometry, which is periodic in the direction parallel to the surface but is *not* periodic in the perpendicular direction, sandwiched by semi-infinite media, such as vacuum, an electrode, or an electrolyte (see Fig. 1). We will call the medium "effective screening medium" (ESM) hereafter. We treat the slab part that consists of substrate and adsorbate atoms microscopically within DFT; we treat the medium part within a continuum characterized by relative permittivity $\epsilon(\boldsymbol{r})$ and additional classical charge density $\rho_{\mathrm{c}}(\boldsymbol{r})$. As stated in the Introduction, we assume that the electrons are confined to the region, say $z \in [-z_0, z_0]$, and that the wave functions are solved using the repeated slab of length $2z_0$, for which standard DFT-PW-PP programs are applicable.

B. Total-energy functional

The total-energy functional of the ESM model is

$$E[\rho_e, V] = K[\rho_e] + E_{xc}[\rho_e] - \int d\boldsymbol{r} \frac{\epsilon(\boldsymbol{r})}{8\pi} |\nabla V(\boldsymbol{r})|^2 + \int d\boldsymbol{r} [\rho_e(\boldsymbol{r}) + \rho_I(\boldsymbol{r})] V(\boldsymbol{r}), \quad (3)$$

where $\rho_e(\boldsymbol{r})$ denotes the electron charge density, $\rho_I(\boldsymbol{r})$ is the nuclear charge density, and $V(\boldsymbol{r})$ is the electrostatic potential. In addition, K and E_{xc}, respectively, represent the kinetic and exchange-correlation energy functional of the electrons; $\epsilon(\boldsymbol{r})$ is the (nonuniform) relative permittivity of the ESM. In this equation, the classical charge density is omitted for simplicity. We also omit the entropic term of the electrons.[20]

The Kohn-Sham equation is obtained when the total-energy functional is varied by the Kohn-Sham orbital under the orthonormality constraint. When varied by the electrostatic potential, we obtain a Poisson equation, Eq. (1), that differs from an ordinary Poisson equation in that the relative permittivity has a spatial dependence.

Next we rewrite the total-energy functional using a Green's function for the Poisson equation

$$\nabla \cdot [\epsilon(\boldsymbol{r}) \nabla] G(\boldsymbol{r}, \boldsymbol{r}') = -4\pi \delta(\boldsymbol{r} - \boldsymbol{r}'). \quad (4)$$

Equation (3) becomes

$$E[\rho_e] = K[\rho_e] + E_{xc}[\rho_e] + \frac{1}{2} \int\int d\boldsymbol{r} d\boldsymbol{r}' \rho_e(\boldsymbol{r}) G(\boldsymbol{r}, \boldsymbol{r}') \rho_e(\boldsymbol{r}') + \int\int d\boldsymbol{r} d\boldsymbol{r}' \rho_e(\boldsymbol{r}) G(\boldsymbol{r}, \boldsymbol{r}') \rho_I(\boldsymbol{r}') + \frac{1}{2} \int\int d\boldsymbol{r} d\boldsymbol{r}' \rho_I(\boldsymbol{r}) G(\boldsymbol{r}, \boldsymbol{r}') \rho_I(\boldsymbol{r}'), \quad (5)$$

which has the well-known form for the DFT energy functional, except that the electrostatic interaction is modified slightly from $1/r$ to that according to Eq. (4). The third, fourth, and fifth terms, respectively, correspond to Hartree energy (E_H), electron-ion interaction energy ($E_{e\text{-}i}$), and ion-ion interaction energy (E_{ion}). The term for interaction between the electrons and the nuclei

$$\int\int d\boldsymbol{r} d\boldsymbol{r}' \rho_e(\boldsymbol{r}) G(\boldsymbol{r}, \boldsymbol{r}') \rho_I(\boldsymbol{r}'), \quad (6)$$

can be rewritten for the pseudopotential scheme as

$$\int\int d\boldsymbol{r} d\boldsymbol{r}' \rho_e(\boldsymbol{r}) G(\boldsymbol{r}, \boldsymbol{r}') \rho_g(\boldsymbol{r}') + \int d\boldsymbol{r} \rho_e(\boldsymbol{r}) V_{loc}^{short}(\boldsymbol{r}) + \sum_\alpha \langle \phi_\alpha | \Delta V_{ps} | \phi_\alpha \rangle, \quad (7)$$

in which the first, second, and third term correspond, respectively, to the long-range local, short-range local, and nonlocal part.[21] The detailed formulation of the long-range local part will be described in Appendix C. In the first term, $\rho_g(\boldsymbol{r})$ is the effective nucleus charge localized near the nuclear position; $V_{loc}^{short}(\boldsymbol{r})$ is the short-range local potential; ϕ_αs are the Kohn-Sham orbitals; and ΔV_{ps} is the nonlocal part of the pseudopotential, which has a finite range from the nuclear position. We call the sum of the first and second terms the local potential energy (E_{loc}) hereafter.

Here we comment on the transferability of the pseudopotential. Pseudopotentials are constructed using an atom isolated in vacuum. For that reason, they cannot be used for atoms located in the region where the relative permittivity becomes considerably larger than 1. On this basis, we will locate the nuclei in the region of $\epsilon_r = 1$ in our model. In principle, however, it would become possible to construct a pseudopotential by locating the nucleus in a medium of given value for ϵ_r, but that is beyond the scope of this study.

C. Analytical solution of the Poisson equation

This section shows a Green's function formulation for the solution of the Poisson equation Eq. (1), which is accomplished by imposing appropriate boundary conditions on Eqs. (1) and (4), and expressing the solution as

$$V(\boldsymbol{r}) = \int d\boldsymbol{r}' G(\boldsymbol{r}, \boldsymbol{r}') \rho_{tot}(\boldsymbol{r}'). \quad (8)$$

Below we consider some important boundary conditions for which Green's function is determined analytically. [Note that one can alternatively solve the Poisson equation for an arbitrary form of $\epsilon(\boldsymbol{r})$ using a finite-difference approach on a regular grid.[22]] For this purpose we consider the case in which relative permittivity depends only on z. Then the Poisson equation

$$\{\partial_z [\epsilon(z) \partial_z] + \epsilon(z) \nabla_\parallel^2\} G(\boldsymbol{r}_\parallel - \boldsymbol{r}_\parallel', z, z') = -4\pi \delta(\boldsymbol{r}_\parallel - \boldsymbol{r}_\parallel') \delta(z - z'), \quad (9)$$

becomes the following in the Laue representation:

$$\{\partial_z [\epsilon(z) \partial_z] - \epsilon(z) g_\parallel^2\} G(\boldsymbol{g}_\parallel, z, z') = -4\pi \delta(z - z'), \quad (10)$$

where $\boldsymbol{g}_\parallel$ is a wave vector parallel to the surface and $g_\parallel$ indicates the absolute value of $\boldsymbol{g}_\parallel$. Then we consider the following four boundary conditions:

(i) $\partial_z V(\boldsymbol{g}_\parallel, z)|_{z=\pm\infty} = 0$, $\epsilon(z) = 1$;

(ii) $V(\boldsymbol{g}_\parallel, \pm z_1) = 0$, $\epsilon(z) = \begin{cases} 1 & \text{if } |z| \leq z_1 \\ \infty & \text{if } |z| \geq z_1; \end{cases}$

(iii) $\begin{cases} V(\boldsymbol{g}_\parallel, z)|_{z=z_1} = 0 \\ \partial_z V(\boldsymbol{g}_\parallel, z)|_{z=-\infty} = 0 \end{cases}$, $\epsilon(z) = \begin{cases} 1 & \text{if } z \leq z_1 \\ \infty & \text{if } z \geq z_1; \end{cases}$

(iv) $\partial_z V(\boldsymbol{g}_\parallel, z)|_{z=\pm\infty} = 0$, $\epsilon(z) = \begin{cases} 1 & \text{if } |z| \leq z_1 \\ \epsilon_r & \text{if } |z| \geq z_1. \end{cases}$

The boundary condition (i) represents a slab located in the vacuum. This is a special case of the ESM model in which no screening exists. We can easily obtain Green's function from Eq. (10) as

$$G^b(\boldsymbol{g}_\parallel, z, z') = \frac{4\pi}{2g_\parallel} e^{-g_\parallel |z - z'|}. \quad (11)$$

This is equal to the Fourier component of the bare Coulomb

$$G^{\mathrm{b}}(\boldsymbol{r}_{\parallel}-\boldsymbol{r}'_{\parallel},z,z')=\frac{1}{\sqrt{|\boldsymbol{r}_{\parallel}-\boldsymbol{r}'_{\parallel}|^2+(z-z')^2}}. \tag{12}$$

It is noteworthy that the present boundary condition is applicable only to neutral systems because otherwise, either $\partial_z V(0,-\infty)$ or $\partial_z V(0,+\infty)$ should be nonzero, as is well known for the one-dimensional Poisson equation. In that case, $V(0,z)$ has a linear increase or decrease with z, thereby rendering the electrostatic energy divergent. For neutral systems, the calculation with our scheme becomes essentially the same as that with the repeated slab model when a sufficiently long supercell is used for the z direction. However, several important differences exist between the two calculations. When using the boundary condition (i), the electrostatic potential always refers to the vacuum level, whereas such is not the case for the repeated slab calculation; this fact is important when calculating the work function. Even when the slab has a dipole moment and, therefore, $V(0,z)$ has a long tail, no correction is required when using (i), contrary to the repeated slab calculations.[23,24]

Imposing the boundary condition (ii), which will be called "metal/vacuum/metal," on a symmetric slab model, we can calculate the surface to which a separated metal electrode applies a bias voltage. The electrode region, $|z|>z_1$, has infinite relative permittivity and thus should have a constant potential, which is taken to be zero and is used as a reference energy. This system would correspond to the STM experimental setup in which the STM tip is modeled by a metal capacitor: This model would be appropriate when the tip-surface distance is sufficiently large so that overlap in the electronic wave functions can be neglected. We can solve Eq. (10) analytically as

$$G^{(\mathrm{ii})}(\boldsymbol{g}_{\parallel},z,z')=\frac{4\pi}{2g_{\parallel}}e^{-g_{\parallel}|z-z'|}+\frac{4\pi}{2g_{\parallel}}\times\frac{e^{-2g_{\parallel}z_1}\cosh[g_{\parallel}(z-z')]-\cosh[g_{\parallel}(z+z')]}{\sinh(2g_{\parallel}z_1)}, \tag{13}$$

when both z and z' are in the region $|z|<z_1$. This equation consists of the bare Coulomb part (the first term) and the rest (the second term), which can be interpreted as a mirror image part, as can be shown by rewriting the second term as

$$\frac{4\pi}{2g_{\parallel}}\sum_{m=0}^{\infty}\{\exp[-g_{\parallel}(z-z'+(4m+4)z_1)]+\exp[g_{\parallel}(z-z'-(4m+4)z_1)]-\exp[-g_{\parallel}(z+z'+(4m+2)z_1)]-\exp[g_{\parallel}(z+z'-(4m+2)z_1)]\}. \tag{14}$$

That is, the second term represents Coulomb interaction with a series of image charges located at the mirror image positions, $z=-z'\pm(4m+2)z_1$ and $z=z'\pm(4m+4)z_1$.

Here we comment that, with the help of the Green's function technique [Eq. (13)] we can accurately compute the Hartree interaction with the image charges, but not for the exchange-correlation (xc) interaction. Nonlocal electron correlation is known to exist between interacting fragments,[25] which in our case is between the surface and the electrode. The xc interaction is considered to be much weaker than that of the Hartree when the distance is taken to be about 10 Å, a typical surface-tip distance; however, it is an important theme of future research to investigate how the electron-electron interaction would be affected by existence of the image.

In boundary condition (iii), say "vacuum/metal," the metal electrode is put on only one side of the slab, as $z>z_1$. When the slab is constituted by atomic layers, or by atomic chains or a tubular nanomaterial like carbon nanotubes extending to x or y direction, the system correspond to the back gate FET experimental setup in which the metallic continuum that is separately located at $z>z_1$ plays the role of a back gate electrode. By solving Eq. (10) we obtain Green's function as

$$G^{(\mathrm{iii})}(\boldsymbol{g}_{\parallel},z,z')=\frac{4\pi}{2g_{\parallel}}e^{-g_{\parallel}|z-z'|}-\frac{4\pi}{2g_{\parallel}}e^{-g_{\parallel}(2z_1-z-z')}, \tag{15}$$

when both z and z' are smaller than z_1. This equation consists of the bare Coulomb part (the first term) and the mirror image part (the second term). Contrary to the case for the boundary condition (ii), only one image appears at $z=-z'+2z_1$.

By imposing the boundary condition (iv), say "solvent/vacuum/solvent," we can calculate the surface that is in contact with the solution. In regions I and III, which, respectively, correspond to $z<-z_1$ and $z>z_1$, the relative permittivity is taken to be that of the solution; it is 78.4 for water. The philosophy behind this model is identical to that of the polarized continuum model (PCM) (Ref. 26) and its modifications.[18] We can solve Eq. (10) analytically; Green's function is

$$G^{(\mathrm{iv})}_{\mathrm{II}}(\boldsymbol{g}_{\parallel},z,z')=\frac{4\pi}{2g_{\parallel}}e^{-g_{\parallel}|z-z'|}+\frac{4\pi}{2g_{\parallel}}\frac{e^{-2g_{\parallel}z_1}(\epsilon_r-1)^2\cosh[g_{\parallel}(z-z')]-(\epsilon_r^2-1)\cosh[g_{\parallel}(z+z')]}{2\epsilon_r\cosh(2g_{\parallel}z_1)+(1+\epsilon_r^2)\sinh(2g_{\parallel}z_1)}, \tag{16}$$

when both z and z' are in the region II, i.e., within the region $[-z_1,z_1]$. Rewriting the second term on the right-hand side as

$$\frac{4\pi}{2g_{\parallel}}\sum_{m=0}^{\infty}\left[\left(\frac{\epsilon_r-1}{\epsilon_r+1}\right)^{2m+2}\{\exp[-g_{\parallel}(z-z'+(4m+4)z_1)]+\exp[g_{\parallel}(z-z'-(4m+4)z_1)]\}-\left(\frac{\epsilon_r-1}{\epsilon_r+1}\right)^{2m+1}\{\exp[-g_{\parallel}(z+z'+(4m+2)z_1)]+\exp[g_{\parallel}(z+z'-(4m+2)z_1)]\}\right], \quad (17)$$

it is readily apparent that Eq. (16) consists of the bare Coulomb term (the first term) and the image charge part (the second term). The positions of the image charges are identical to those that we found in the case of boundary condition (ii), but the interaction decreases exponentially as the distance from the image increases.

We must impose the charge neutrality condition on the system, as in the case of boundary condition (i). In a solution, however, electrolyte ions such as H^+ or SO_4^{2-} exist and can change their spatial distributions to screen the electrostatic potential. For that reason, the whole system is always neutral, even when the surface is charged up. The screening length ranges from nanometers to micrometers depending on the ion density. In addition, its atomic scale description is too demanding. For those reasons, we incorporate the screening effect macroscopically using a continuum model. As the continuum model, we use modified PB (MPB) theories,[27] the detailed formulation of which will be given in the Appendix A. Thereby, we can treat the charged surfaces in the solution within the boundary condition (iv).

It is noteworthy that the electrostatic potential obtained by Eq. (8) is not periodic in the cell $[-z_0, z_0]$ and must be made periodic for use for the Kohn-Sham solver. For this, we modify the potential near the cell boundary, where the electron density is negligibly small.[28] It is convenient to use a cubic polynomial for this purpose.

D. Constant-μ calculation

The zero of the electrostatic potential constitutes the base relative to which levels, ε_α, and the chemical potential of electrons, μ, are determined. For electrons in the grand canonical ensemble, the density is then obtained as

$$\rho_e(\boldsymbol{r}) = \sum_{\alpha}^{\varepsilon_\alpha \leq \mu} |\phi_\alpha(\boldsymbol{r})|^2 \quad (18)$$

on the basis of the energy level of the Kohn-Sham orbital, which is calculated from

$$\left[-\frac{1}{2}\nabla^2 + V(\boldsymbol{r}) + V_{xc}(\boldsymbol{r};\rho_e)\right]\phi_\alpha(\boldsymbol{r}) = \varepsilon_\alpha \phi_\alpha(\boldsymbol{r}), \quad (19)$$

where $V_{xc}(\boldsymbol{r})$ is the exchange-correlation potential. In this procedure, the total number of electrons, N_e, is not given in advance. It is instead determined through self-consistent calculations. From this constant-μ scheme, we can obtain the grand potential as a function of μ, which enables us to discuss thermodynamic stability of a surface phase, as was emphasized in Ref. 14. In practice, one can use Eq. (18) at every self-consistent loop (constant-μ mode). Alternatively, one can do several parallel calculations for given values for N_e (constant-N_e mode) from which the grand potential is obtained through interpolation. The former is usually less stable and requires more iterations to achieve self-consistency.

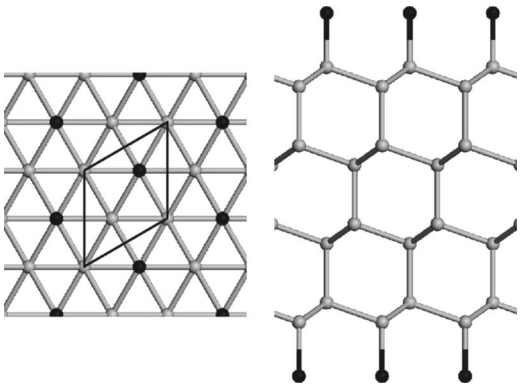

FIG. 2. Top view (left panel) and side view (right panel) of the Al/Si(111) slab model. Gray and black balls, respectively, represent Si and Al atoms. The solid line denotes the unit cell of the surface.

III. APPLICATION TO A PRACTICAL CALCULATION

In Sec. II, we presented several Green's functions that were obtained by imposing boundary conditions (i)–(iv). Their simple analytic form allows us to obtain the electrostatic potential very easily, similarly to the case of the repeated slab calculations. This ease in obtaining them makes it feasible to perform first-principles calculations of the surfaces while imposing various boundary conditions. This section presents a simple benchmark calculation using Al/Si(111) to demonstrate the applicability of our method.

The surface has a symmetric slab structure, as shown in Fig. 2. The Si slab has 1×1 lateral periodicity and is eight atomic layers thick. The Al atoms are adsorbed on the on-top site. The lattice parameter and the Si-Al distance are 5.43 Å and 2.15 Å, respectively. Thickness of the vacuum region, ℓ_{vac}, is 10 Å. All calculations are performed using the generalized gradient approximation (GGA) within the DFT.[1,2] We use the Perdew-Burke-Ernzerhof (PBE)-type exchange-correlation functional.[29,30] Norm-conserving pseudopotentials with separable form are adopted to describe electron-ion interaction.[31,32] The valence wave functions are expanded by the planewave basis set with a cut-off energy, E_{cut}, of 16 Ryd. The number of sampled k points in the irreducible Brillouin zone is 12. We use the computer code TOKYO AB-INITIO PROGRAM PACKAGE (TAPP),[33] in which the ESM part is newly implemented.

A. Proof test

In boundary condition (i), where the relative permittivity of the ESM is 1, Al/Si(111) is embedded in vacuum. This corresponds to a repeated slab model with sufficiently large ℓ_{vac}. As a proof-test, we compute the total energy and the energy terms in Eq. (5) for both the ESM and the repeated

TABLE I. Comparison of energies in Eq. (5) calculated for Al/Si(111). RS and BC(i), respectively, denote the repeated slab calculation and the calculation with the boundary condition (i). The energy unit is Hartree.

	K	E_{xc}	E_H	E_{loc}	E_{ion}	E_{tot}
RS	13.6359	−11.0195	112.8645	−228.4642	77.5645	−35.4188
BC(i)	13.6359	−11.0195	−952.9827	1893.1658	−978.2183	−35.4188

slab (ℓ_{vac}=10 Å). As shown in Table I, K and E_{xc} are identical within an accuracy of 0.1 mHartree, indicating that the electronic wave functions and the electron density are fundamentally identical in both calculations. Although the values for E_H, E_{loc}, and E_{ion} are different because of different treatment for the diverging term, i.e., $\boldsymbol{g}_{\parallel}=0$ term, the total energies, E_{tot}, are identical in both calculations. The residual difference in E_{tot}, a few hundredths of a mHartree (not shown in the table), is originated from the different definitions of the cut-off energy; it is conventionally defined as $\frac{1}{2}|\boldsymbol{G}|^2 \leqslant E_{cut}$, but in our case as $\frac{1}{2}|\boldsymbol{G}_{\parallel}|^2 \leqslant E_{cut}$, because the ESM calculation is based on the Laue representation. The difference will become negligible if we use an extremely large value for the cutoff.

The atomic force is calculable using the analytic derivative of the total energy. We have checked that the force is calculated accurately. The computational time to obtain the force was found to be almost identical to that for the repeated slab calculation.

B. "Metal/vacuum/metal" and "vacuum/metal"

Now that we have tested the ESM implementation using the boundary condition (i), let us proceed to other boundary conditions (ii) and (iii), i.e., the surface located near the metallic electrode. We can perform the calculation at constant-N_e mode or at constant-μ mode, but the former is generally faster because of its more rapid SCF convergence. Here we present the calculation in the constant-N_e mode in which the charge state is taken as $\pm 0.01e$, $\pm 0.005e$, and $0e$ per unit cell.

Figures 3(a) and 3(b) show the geometry of our model. The ESM (electrode in the present case) is located at $|z| > z_1$ for the boundary condition (ii) and $z > z_1$ for the boundary condition (iii), where z_1 is taken to be away from the Al layer by 10 Å. Carefully checking the tail of the electronic wave function ϕ, we determine the position for z_0 beyond which ϕ has negligibly small amplitude. Then the Kohn-Sham equation is solved by applying the periodic boundary condition at $|z|=z_0$.

First we show results for the boundary condition (ii), metal/vacuum/metal. Figures 3(c) and 3(e), respectively, show the planar average of the valence charge density, $\Delta\rho$, and the electrostatic potential, ΔV, in reference to those of the neutral surface. As shown in Fig. 3(c), the electron accumulates or depletes around the Al layer, but not in the Si layers; consequently, metallic screening occurs at the Al layer. This feature is also apparent in Fig. 3(e), where ΔV is almost flat in the Si layers; it bends only near the Al layer. By calculating the gradient of V in the vacuum region, we can obtain the strength of the electric field near the surface. The results are −0.071, −0.036, 0.035, and 0.071 V/Å for the charge states of $+0.01e$, $+0.005e$, $-0.005e$, and $-0.01e$, respectively. Figures 3(d) and 3(f), respectively, show $\Delta\rho$ and ΔV calculated with the boundary condition (iii), vacuum/

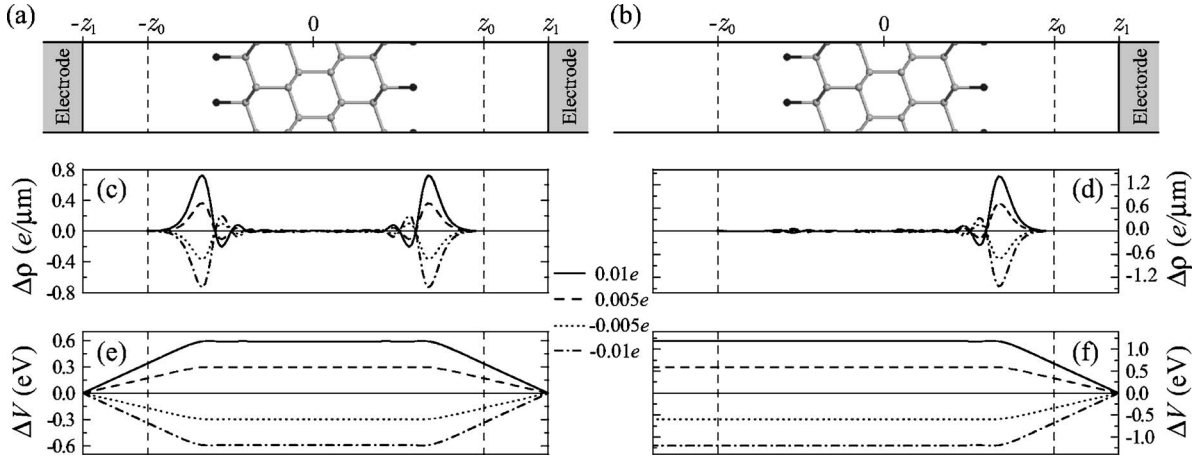

FIG. 3. Side view of the Al/Si(111) slab model (a) with boundary condition (ii) and (b) with boundary condition (iii). Gray and black balls, respectively, represent Si and Al atoms. Gray areas indicate the ESM (electrode). Both z_0 and z_1 indicate the cell boundary for the repeated slab calculation and electrode position, respectively. The planar average of the valence charge density $\Delta\rho$ (see text) is calculated with (c) boundary condition (ii) and (d) boundary condition (iii). The planar average of the electrostatic potential ΔV (see text) is calculated with (e) boundary condition (ii) and (f) boundary condition (iii). Solid, broken, dotted, dashed-dotted lines, respectively, denote $+0.01e$, $+0.005e$, $-0.005e$, and $-0.01e$ surface charge states.

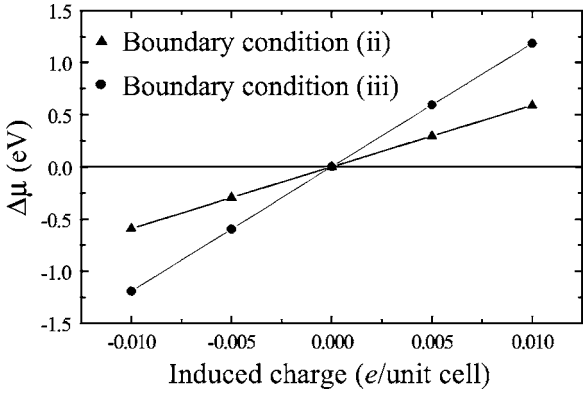

FIG. 4. Fermi energy difference $\Delta\mu$ with respect to that of the neutral surface as a function of the induced charge on the surface. Triangles and circles denote the calculation with boundary condition (ii) and (iii), respectively.

metal. Contrary to the boundary condition (ii), the metal electrode is placed only at the right-hand side of the slab [see Fig. 3(b)].

In the present method, the bias applied to the surface is obtainable as the difference in the Fermi energy between the charged system and the neutral system. Figure 4 shows the applied bias plotted against the induced electrons on the surface. Reflecting the two-dimensionality of the local density of states around the surface, the bias is linearly dependent on the induced charge. The slope for the boundary condition (ii) is almost half of that for the boundary condition (iii). This can be understood from the facts that charge is induced on both sides for the boundary condition (ii) whereas it is induced on only one side for the boundary condition (iii) and that the induced charges become almost equal when summed up on both sides. Roughly estimated from Fig. 4, one electron per 100 surface sites is induced on the surface when applied with the bias of 1 V.

C. Solvent-metal interface

Let us now examine the ESM model combined with macroscopic theory for the solution. For macroscopic theory, we use the MPB theory.[27] Note that, when using a finite value for the relative permittivity for the ESM, we must introduce a neutralizing charge to prevent divergence in the electrostatic energy of the charged surfaces.

As discussed in Appendix A, the MPB modifies the original PB theory by introducing an effective expulsion radius to account for the steric effect. Since the electrolyte ion density $\rho_c(\boldsymbol{r})$ depends nonlinearly on the electrostatic potential $V(\boldsymbol{r})$, $\rho_c(\boldsymbol{r})$, and $V(\boldsymbol{r})$ need to be solved self-consistently through iteration, but because the functional $\rho_c[V]$ has a very simple analytical form (see Appendix A), they can be determined within inconsequential CPU time.

The system geometry is shown in Fig. 5(a), where only the region of positive z is shown because we are using a symmetric slab. In the present calculation, we use the MPB parameters as follows. The expulsive volume of the ion is $v=7.5^3$ Å^3 both for cation and anion; both ions has the valence of 1 and bulk density of 0.1 M; the temperature is

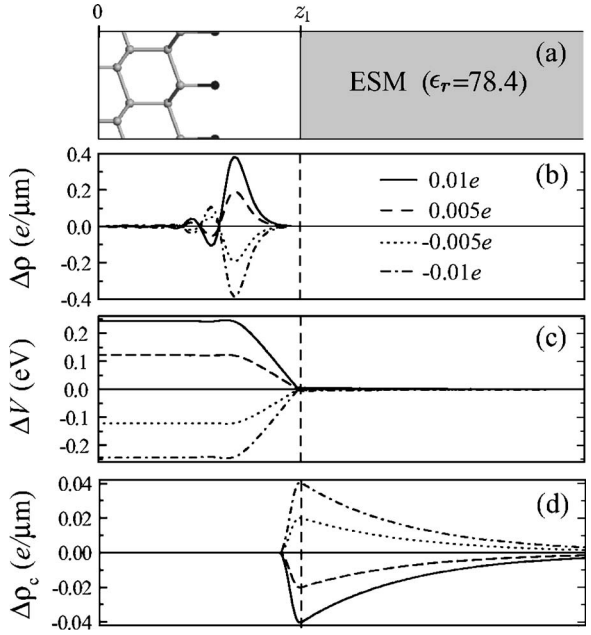

FIG. 5. (a) Side view of the Al/Si(111) slab model with boundary condition (iv). Gray and black balls indicate Si and Al atoms, respectively. Gray areas indicate the ESM (water); z_1 indicates the cell boundary for the repeated slab calculation. The planar average of (b) $\Delta\rho$, (c) ΔV, and (d) $\Delta\rho_c$ (see text). Solid, broken, dotted, dashed-dotted lines, respectively, denote $+0.01e$, $+0.005e$, $-0.005e$, and $-0.01e$ surface charge states.

300 K; the Stern layer thickness is 5 Å; and the relative permittivity of the ESM is 78.4. The surface-ESM distance is taken to be 5 Å. The Poisson equation is solved using a cell whose length in the z direction is $4z_0$ (see Appendix A). For charge state calculations, we use $\pm 0.01e$, $\pm 0.005e$, and $0e$ per unit cell.

The planar average of the valence charge density, $\Delta\rho$, the electrostatic potential, $V(\boldsymbol{r})$, and the electrolyte ion density, $\rho_c(\boldsymbol{r})$, are shown respectively in Figs. 5(b)–5(d). The bias voltage applied to the surface is found to be −0.24, −0.12, 0.12, and 0.24 V, respectively, for the charge states of $+0.01e$, $+0.005e$, $-0.005e$, and $-0.01e$. These values correspond to one induced electron per approximately 50 surface sites when applied with the bias voltage of 1 V, which is about two times greater than that obtained above using the boundary condition (ii), where the surface-ESM distance was taken to be 10 Å.

IV. SUMMARY AND PERSPECTIVE

We have proposed a new first-principles computational approach to a surface/interface in the slab model. In view of the fact that the DFT-planewave(PW)-pseudopotential(PP) scheme has been widely applied to surface problems, but that there are problems whose application has been restricted by the periodic boundary condition (PBC) required by the scheme, we modified the scheme so that the PBC requirement might be removed in the surface normal direction. That task was accomplished by making use of the properties of the electrons; the wave function decays rapidly with distance

from the surface. This characteristic allows the use of separate treatments; the Poisson equation is solved in the whole space under study with the help of Green's function technique, whereas the Kohn-Sham equation is solved using a repeated slab of finite length. Using this scheme, we can treat the nonperiodic slab with minimal modification of the DFT-PW-PP scheme. The only parts that must be modified are the Hartree potential, ion core pseudopotential, and the ion-ion interaction.

We have applied the scheme to a slab that is sandwiched by vacuum and/or the effective screening medium (ESM) characterized by relative permittivity, $\epsilon(\boldsymbol{r})$, and additional classical charge density. For the $\epsilon(\boldsymbol{r})$ of ESM, we used infinity to model the STM tip and back gate electrode, and the value 78.4 to model the solution. For the additional classical charge, we used the continuum charge of the modified PB theory to model electrolyte ions in the solution. Using these ESMs, we have performed the calculation for Al/Si(111) in contact with the vacuum, the model STM tip, the model back gate electrode, or the model solution. Then we have discussed the potential profile and induced surface charge. Results of calculations indicated that the computational time required to obtain the electronic structures and the atomic force is almost equal to that of the standard DFT-PW-PP scheme. In this scheme, atomic forces are obtained from the analytic derivative of the total energy. For that reason, this scheme is advantageous for conducting a molecular dynamics simulation conserving the total energy accurately.

Considering the easy implementation and flexibility of our scheme, we consider that the scheme might be modified for wider applications and might be improved through the use of more realistic continuum models.

ACKNOWLEDGMENTS

M.O. would like to thank Y. Yoshimoto (ISSP) and K. Akagi (University of Tokyo) for useful discussions. Computations were done at the ISSP Supercomputer Center, University of Tokyo. This work was partly supported by a Grant-in-Aid for Scientific Research from the Ministry of Education, Culture, Sports, Science and Technology of Japan under Contract No. 16740169.

APPENDIX A: MODIFIED POISSON-BOLTZMANN METHOD

One of the most widely used macroscopic models for electrolyte ions is the Poisson-Boltzmann (PB) model,[15] in which the electrolyte ion distributes statistically according to the electrostatic potential. This model lacks statistical correlations and the steric effect: repulsion between ions. Because of the latter fact, although the model has been successful in predicting ion profiles close to *neutral* surfaces, it strongly overestimates ionic concentrations that are found close to *charged* surfaces. The steric effect is known to be incorporated effectively by introducing the Stern layer,[34] beyond which the ions cannot approach, and more systematically by introducing an effective ionic radius, as was shown recently by Borukhov *et al.*[27] The modified PB (MPB) model has a free-energy form that can be easily combined with our effective screening medium (ESM) scheme.

The MPB introduces number densities of ions, $c_+(\boldsymbol{r})$ and $c_-(\boldsymbol{r})$ for the cation and anion, respectively. They have electrostatic contribution to the free energy as

$$\int d\boldsymbol{r}[z_{\mathrm{ion}}c_-(\boldsymbol{r}) - c_+(\boldsymbol{r})]V(\boldsymbol{r}) - \int d\boldsymbol{r}[\mu_+c_+(\boldsymbol{r}) + \mu_-c_-(\boldsymbol{r})], \tag{A1}$$

where z_{ion} is the valence of the anion; the cation is assumed to be monovalent; μ_+ and μ_- are the chemical potentials of the cation and anion, respectively.[35] They also have the entropic contribution as

$$-TS = \frac{k_BT}{v}\int d\boldsymbol{r}\{vc_+(\boldsymbol{r})\ln[vc_+(\boldsymbol{r})] + vc_-(\boldsymbol{r})\ln[vc_-(\boldsymbol{r})] + [1 - vc_+(\boldsymbol{r}) - vc_-(\boldsymbol{r})]\ln[1 - vc_+(\boldsymbol{r}) - vc_-(\boldsymbol{r})]\}, \tag{A2}$$

where v denotes the effective exclusion volume of the ions and k_BT is the thermal energy. These terms can be added simply to Eq. (3) to obtain the free-energy for our MPB-ESM model. By varying with respect to the ion densities we can obtain the Poisson equation

$$\nabla\cdot[\epsilon(\boldsymbol{r})\nabla]V(\boldsymbol{r}) = -4\pi[\rho_{\mathrm{e}}(\boldsymbol{r}) + \rho_{\mathrm{I}}(\boldsymbol{r}) + z_{\mathrm{ion}}c_-(\boldsymbol{r}) - c_+(\boldsymbol{r})],$$

$$c_-(\boldsymbol{r}) = c_-^0\frac{e^{-z_{\mathrm{ion}}\beta V(\boldsymbol{r})}}{1 - c_-^0v(z_{\mathrm{ion}}+1) + c_-^0v(e^{-\beta z_{\mathrm{ion}}V(\boldsymbol{r})} + z_{\mathrm{ion}}e^{\beta V(\boldsymbol{r})})},$$

$$c_+(\boldsymbol{r}) = c_-^0\frac{z_{\mathrm{ion}}e^{\beta V(\boldsymbol{r})}}{1 - c_-^0v(z_{\mathrm{ion}}+1) + c_-^0v(e^{-\beta z_{\mathrm{ion}}V(\boldsymbol{r})} + z_{\mathrm{ion}}e^{\beta V(\boldsymbol{r})})}, \tag{A3}$$

where c_-^0 is the number density of anion in the bulk. The charge densities of the cation and anion are called the classical charge density, $\rho_{\mathrm{c}}(\boldsymbol{r}) = z_{\mathrm{ion}}c_-(\boldsymbol{r}) - c_+(\boldsymbol{r})$, in the text. The classical charge density must be solved self-consistently because of the nonlinear structure of the equation.

In solving this equation, because the ion densities are much more extended in z direction compared to the densities for the electrons and nuclei, we must use a much larger cell. Even when using such a larger cell, the computational cost for solving the Poisson equation is usually much smaller than that for the Kohn-Sham equation.

APPENDIX B: ION-ION CONTRIBUTION

The ion-ion interaction energy, E_{ion}, in Eq. (5) is usually calculated using Ewald summation method.[36] In our method, however, the electrostatic interaction is modified slightly from $1/r$ because of the presence of the ESM. Let us now reformulate the Ewald summation method to be suitable for the boundary condition (ii) as a representative of our method.

The explicit form of E_{ion} is

$$E_{\mathrm{ion}} = \sum_{\boldsymbol{R}_\parallel \boldsymbol{R}'_\parallel} \sum_{\mu\nu} \frac{Z_\mu Z_\nu}{2} \int\int d\boldsymbol{r} d\boldsymbol{r}'\, \delta(\boldsymbol{r} - \boldsymbol{R}_{\parallel\mu}) \times G^{(\mathrm{ii})}(\boldsymbol{r}_\parallel - \boldsymbol{r}'_\parallel, z, z')\, \delta(\boldsymbol{r}' - \boldsymbol{R}'_{\parallel\nu}) - E_{\mathrm{self}}, \tag{B1}$$

where Z_μ indicates the bare ionic charges of the μth atom (pseudocharges in a PW-PP framework); $\boldsymbol{R}_{\parallel\mu}$ is an abbreviated notation of μth atom in a unit cell, i.e., $\boldsymbol{R}_\parallel + \boldsymbol{\tau}_\mu$, and E_{self} is the self-interaction correction term which is defined as

$$E_{\mathrm{self}} = \sum_{\boldsymbol{R}_\parallel} \sum_{\mu} \frac{Z_\mu^2}{2} \int\int d\boldsymbol{r} d\boldsymbol{r}'\, \delta(\boldsymbol{r} - \boldsymbol{R}_{\parallel\mu}) \times G^{\mathrm{b}}(\boldsymbol{r}_\parallel - \boldsymbol{r}'_\parallel, z, z')\, \delta(\boldsymbol{r}' - \boldsymbol{R}_{\parallel\mu}). \tag{B2}$$

By introducing a fictitious Gaussian charge distribution

$$\rho_{\mathrm{fic}}(\boldsymbol{r} - \boldsymbol{R}_{\parallel\mu}) = \frac{Z_\mu \eta^3}{\pi^{3/2}} e^{-\eta^2 |\boldsymbol{r} - \boldsymbol{R}_{\parallel\mu}|^2}, \tag{B3}$$

we can split the first term of Eq. (B1) into two parts as $E_{\mathrm{G}} + E_{\mathrm{R}}$, where these two parts are defined as

$$E_{\mathrm{G}} = \sum_{\boldsymbol{R}_\parallel \boldsymbol{R}'_\parallel} \sum_{\mu\nu} \frac{Z_\mu Z_\nu}{2} \int\int d\boldsymbol{r} d\boldsymbol{r}'\, \delta(\boldsymbol{r} - \boldsymbol{R}_{\parallel\mu}) \times G^{(\mathrm{ii})}(\boldsymbol{r}_\parallel - \boldsymbol{r}'_\parallel, z, z')\, \rho_{\mathrm{fic}}(\boldsymbol{r}' - \boldsymbol{R}'_{\parallel\nu}), \tag{B4}$$

$$E_{\mathrm{R}} = \sum_{\boldsymbol{R}_\parallel \boldsymbol{R}'_\parallel} \sum_{\mu\nu} \frac{Z_\mu Z_\nu}{2} \int\int d\boldsymbol{r} d\boldsymbol{r}'\, \delta(\boldsymbol{r} - \boldsymbol{R}_{\parallel\mu}) \times G^{(\mathrm{ii})}(\boldsymbol{r}_\parallel - \boldsymbol{r}'_\parallel, z, z')[\delta(\boldsymbol{r}' - \boldsymbol{R}'_{\parallel\nu}) - \rho_{\mathrm{fic}}(\boldsymbol{r}' - \boldsymbol{R}'_{\parallel\nu})]. \tag{B5}$$

The η in Eq. (B3) is an arbitrary parameter, whose value ensures good convergence of both sums over $\boldsymbol{G}_\parallel$ and $\boldsymbol{R}_\parallel$ space, where $\boldsymbol{G}_\parallel$ is a reciprocal-lattice vector parallel to the surface.

After straightforward calculations, we obtain

$$E_{\mathrm{G}} = \sum_{\boldsymbol{G}_\parallel \neq 0} \sum_{\mu\nu} \frac{Z_\mu Z_\nu}{2S_0} e^{i\boldsymbol{G}_\parallel \cdot (\boldsymbol{\tau}_{\mu\parallel} - \boldsymbol{\tau}_{\nu\parallel})} [F_1^\eta(\boldsymbol{G}_\parallel, \tau_\mu^z, \tau_\nu^z) + F_2(\boldsymbol{G}_\parallel, \tau_\mu^z, \tau_\nu^z)] + \sum_{\mu\nu} \frac{\pi Z_\mu Z_\nu}{S_0} \left[\left(z_1 - \frac{\tau_\mu^z \tau_\nu^z}{z_1} \right) - (\tau_\mu^z - \tau_\nu^z) \mathrm{erf}[\eta(\tau_\mu^z - \tau_\nu^z)] - \frac{1}{\eta\sqrt{\pi}} e^{-\eta^2 (\tau_\mu^z - \tau_\nu^z)^2} \right], \tag{B6}$$

where $\mathrm{erf}(x)$ is the error function; S_0 is the area of the surface unit cell; and the functions F_1 and F_2 are defined as

$$F_1^\eta(\boldsymbol{G}_\parallel, \tau_\mu^z, \tau_\nu^z) = \frac{\pi}{G_\parallel} \left\{ e^{-G_\parallel (\tau_\mu^z - \tau_\nu^z)} \,\mathrm{erfc}\left[\frac{G_\parallel}{2\eta} - \eta(\tau_\mu^z - \tau_\nu^z) \right] + e^{G_\parallel (\tau_\mu^z - \tau_\nu^z)} \,\mathrm{erfc}\left[\frac{G_\parallel}{2\eta} + \eta(\tau_\mu^z - \tau_\nu^z) \right] \right\}, \tag{B7}$$

$$F_2(\boldsymbol{G}_\parallel, \tau_\mu^z, \tau_\nu^z) = \frac{2\pi}{G_\parallel} \frac{e^{-2G_\parallel z_1} \cosh[G_\parallel(\tau_\mu^z - \tau_\nu^z)] - \cosh[G_\parallel(\tau_\mu^z + \tau_\nu^z)]}{\sinh(2G_\parallel z_1)}, \tag{B8}$$

where $\mathrm{erfc}(x)$ is the complementary error function and $G_\parallel$ indicates the absolute value of $\boldsymbol{G}_\parallel$.

When we calculate Eq. (B5), we should note the following. The image charge from the point charge located at $\boldsymbol{R}_{\parallel\nu}$ and that from the Gaussian charge located at $\boldsymbol{R}_{\parallel\nu}$ are identical unless the tail of the Gaussian charge and the ESM overlap each other.[37] Therefore it is easy to show that the electrostatic potential from those image charges has no contribution to E_{R}. Thanks to this fact, we can only calculate the bare Coulomb term in Eq. (B5) without evaluating a slowly convergent series [see Eq. (14)]. Then we can rewrite E_{R} as

$$E_{\mathrm{R}} = \sum_{\boldsymbol{R}_\parallel \boldsymbol{R}'_\parallel} \sum_{\mu\nu} \frac{Z_\mu Z_\nu}{2} \int\int d\boldsymbol{r} d\boldsymbol{r}'\, \delta(\boldsymbol{r} - \boldsymbol{R}_{\parallel\mu}) G^{\mathrm{b}}(\boldsymbol{r}_\parallel - \boldsymbol{r}'_\parallel, z, z') \times [\delta(\boldsymbol{r}' - \boldsymbol{R}'_{\parallel\nu}) - \rho_{\mathrm{fic}}(\boldsymbol{r}' - \boldsymbol{R}'_{\parallel\nu})] = \sum_{\boldsymbol{R}_\parallel} \sum_{\mu\nu} \frac{Z_\mu Z_\nu}{2} \frac{\mathrm{erfc}(\eta |\boldsymbol{R}_{\parallel\mu} + \boldsymbol{\tau}_\mu - \boldsymbol{\tau}_\nu|)}{|\boldsymbol{R}_{\parallel\mu} + \boldsymbol{\tau}_\mu - \boldsymbol{\tau}_\nu|}. \tag{B9}$$

A divergent term in E_{R} is canceled by that in E_{self}. Finally we obtain the ion-ion interaction energy as

$$E_{\mathrm{ion}} = \sum_{\boldsymbol{R}_\parallel} \sum_{\mu\nu} \frac{Z_\mu Z_\nu}{2} \frac{\mathrm{erfc}(\eta |\boldsymbol{R}_{\parallel\mu} + \boldsymbol{\tau}_\mu - \boldsymbol{\tau}_\nu|)}{|\boldsymbol{R}_{\parallel\mu} + \boldsymbol{\tau}_\mu - \boldsymbol{\tau}_\nu|} - \sum_\mu Z_\mu^2 \frac{\eta}{\sqrt{\pi}} + \sum_{\boldsymbol{G}_\parallel \neq 0} \sum_{\mu\nu} \frac{Z_\mu Z_\nu}{2S_0} e^{i\boldsymbol{G}_\parallel \cdot (\boldsymbol{\tau}_{\mu\parallel} - \boldsymbol{\tau}_{\nu\parallel})} [F_1^\eta(\boldsymbol{G}_\parallel, \tau_\mu^z, \tau_\nu^z) + F_2(\boldsymbol{G}_\parallel, \tau_\mu^z, \tau_\nu^z)] + \sum_{\mu\nu} \frac{\pi Z_\mu Z_\nu}{S_0} \left[\left(z_1 - \frac{\tau_\mu^z \tau_\nu^z}{z_1} \right) - (\tau_\mu^z - \tau_\nu^z) \mathrm{erf}[\eta(\tau_\mu^z - \tau_\nu^z)] - \frac{1}{\eta\sqrt{\pi}} e^{-\eta^2 (\tau_\mu^z - \tau_\nu^z)^2} \right], \tag{B10}$$

where the sum over $\boldsymbol{R}_\parallel$ excludes $\boldsymbol{R}_\parallel + \boldsymbol{\tau}_\mu - \boldsymbol{\tau}_\nu = 0$.

APPENDIX C: LOCAL IONIC PSEUDOPOTENTIAL

In a PW-PP scheme, the term for an interaction between electrons and effective nucleus charge (pseudocharge) is decomposed into two parts: a local part and a nonlocal part [the third term of Eq. (7)]. In the evaluation of the local part, it is often convenient to separate the local part into two parts: a long-range local part [the first term of Eq. (7)] and a short-range local part [the second term of Eq. (7)]. For the short-range local part and the nonlocal part, we can use conventional pseudopotential generation schemes. On the other hand, it is necessary to change the generation method for the long-range local part as indicated below.

The long-range local potential is thought of as originating from Gaussian-type pseudocharges,

$$\rho_{\rm ps}^{\mu}(\boldsymbol{r}) = \sum_{j=1}^{2} \frac{Z_\mu \beta_j^\mu (\alpha_j^\mu)^3}{\pi^{3/2}} e^{-(\alpha_j^\mu)^2 |\boldsymbol{r}|^2}, \tag{C1}$$

where μ is an atom index, $\beta_1^\mu + \beta_2^\mu = 1$, and α_j^μ is a decay constant that is defined during pseudopotential generation. Our method uses two Gaussian components to mimic the effective core charge, as is done in Bachelet, Hamann, and Schlüter (BHS) pseudopotentials.[38] In the present method, electrostatic interaction is slightly modified from $1/r$. For that reason, we must reformulate the interaction between the electrons and the pseudocharge. Because the ESM is located at far from the surface outside the range of the short-range part and the nonlocal part, only the long-range local part should be modified by applying Green's function to above $\rho_{\rm ps}^{\mu}(\boldsymbol{r})$.

Here we show the long-range local potential, $V_{\rm loc}^{\rm long}(\boldsymbol{g}_\parallel, z)$, for the boundary condition (ii) as a representative of our method. Starting from Eq. (8) in $\boldsymbol{g}_\parallel$ space,

$$V_{\rm loc}^{\rm long}(\boldsymbol{g}_\parallel, z) = \int_{-z_1}^{z_1} dz' G^{\rm (ii)}(\boldsymbol{g}_\parallel, z, z') \rho_{\rm g}(\boldsymbol{g}_\parallel, z'), \tag{C2}$$

where $\rho_{\rm g}(\boldsymbol{r})$ is the effective core charge given by

$$\rho_{\rm g}(\boldsymbol{r}_\parallel, z) = \sum_{\boldsymbol{R}_\parallel} \sum_{\mu} \rho_{\rm ps}^{\mu}(\boldsymbol{r}_\parallel - \boldsymbol{R}_{\parallel\mu}, z - \tau_\mu^z), \tag{C3}$$

in real space, after straightforward calculations, we obtain

$$V_{\rm loc}^{\rm long}(\boldsymbol{g}_\parallel \neq 0, z) = \sum_{\mu} \frac{Z_\mu}{S_0} e^{-i\boldsymbol{g}_\parallel \cdot \boldsymbol{\tau}_{\mu\parallel}} \left[\sum_{j}^{2} \beta_j^\mu F_1^{\alpha_j^\mu}(\boldsymbol{g}_\parallel, z, \tau_\mu^z) + F_2(\boldsymbol{g}_\parallel, z, \tau_\mu^z) \right], \tag{C4}$$

$$V_{\rm loc}^{\rm long}(\boldsymbol{g}_\parallel = 0, z) = -\sum_{\mu} \frac{2\pi Z_\mu}{S_0} \sum_{j=1}^{2} \beta_j^\mu \left[(z - \tau_\mu^z) \mathrm{erf}[\alpha_j^\mu (z - \tau_\mu^z)] + \frac{1}{\alpha_j^\mu \sqrt{\pi}} e^{-(\alpha_j^\mu)^2 (z - \tau_\mu^z)^2} \right] + \sum_{\mu} \frac{2\pi Z_\mu}{S_0} \left(z_1 - \frac{z \tau_\mu^z}{z_1} \right). \tag{C5}$$

[1] P. Hohenberg and W. Kohn, Phys. Rev. **136**, B864 (1964).
[2] W. Kohn and L. J. Sham, Phys. Rev. **140**, A1133 (1965).
[3] See, for example, R. M. Martin, *Electronic Structure* (Cambridge University Press, Cambridge, 2004).
[4] S. K. Desai, V. Pallassana, and M. Neurock, J. Phys. Chem. B **105**, 9171 (2001).
[5] Y. Okamoto, O. Sugino, Y. Mochizuki, T. Ikeshoji, and Y. Morikawa, Chem. Phys. Lett. **377**, 236 (2003).
[6] S. K. Desai and M. Neurock, Phys. Rev. B **68**, 075420 (2003).
[7] K. Hirose and M. Tsukada, Phys. Rev. Lett. **73**, 150 (1994).
[8] N. D. Lang, Phys. Rev. B **52**, 5335 (1995).
[9] Y. Q. Xue, S. Datta, and M. A. Ratner, Chem. Phys. **281**, 151 (2002).
[10] J. Neugebauer and M. Scheffler, Surf. Sci. **287-288**, 572 (1993).
[11] P. J. Feibelman, Phys. Rev. B **64**, 125403 (2001).
[12] K.-M. Ho, B. N. Harmon, and S. H. Liu, Phys. Rev. Lett. **44**, 1531 (1980).
[13] C. L. Fu and K.-M. Ho, Phys. Rev. Lett. **63**, 1617 (1989).
[14] A. Y. Lozovoi, A. Alavi, J. Kohanoff, and R. M. Lynden-Bell, J. Chem. Phys. **115**, 1661 (2001).
[15] G. Gouy, J. Phys. (France) **9**, 457 (1910); Ann. Phys. (Paris) **7**, 129 (1917); D. L. Chapman, Philos. Mag. **25**, 475 (1913).
[16] A. Laio, J. VandeVondele, and U. Rothlisberger, J. Chem. Phys. **116**, 6941 (2002).
[17] Q. J. Cui, J. Chem. Phys. **117**, 4720 (2002).
[18] See, for example, J. Tomasi, B. Mennucci, and R. Cammi, Chem. Rev. (Washington, D.C.) **105**, 2999 (2005).
[19] A. Kovalenko and F. Hirata, J. Chem. Phys. **110**, 10095 (1999).
[20] See, for example, R. G. Parr and W. Yang, *Density-Functional Theory of Atoms and Molecules* (Oxford University Press, New York, 1989), Sec. 9.1.
[21] Strictly speaking, the electrostatic interaction Eq. (6) plus the valence-core exchange-correlation interaction are rewritten as Eq. (7) in the pseudopotential scheme, with the latter interaction being included in the short-range local and the nonlocal parts.
[22] J. Fattebert and F. Gygi, J. Comput. Chem. **23**, 662 (2002).
[23] J. Neugebauer and M. Scheffler, Phys. Rev. B **46**, 16067 (1992).
[24] L. Bengtsson, Phys. Rev. B **59**, 12301 (1999).
[25] H. Rydberg, B. I. Lundqvist, D. C. Langreth, and M. Dion, Phys. Rev. B **62**, 6997 (2000).
[26] S. Miertuš, E. Scorocco, and J. Tomasi, J. Chem. Phys. **55**, 117 (1981).
[27] I. Borukhov, D. Andelman, and H. Orland, Phys. Rev. Lett. **79**, 435 (1997).
[28] We should note the following fact. The total energy of the system is calculated by Eq. (5), whose electrostatic contribution is expressed using the solution of the Poisson equation $V(\boldsymbol{r})$, Eq. (8), and the total charge density $\rho_{\rm tot}(\boldsymbol{r})$ as $\int d\boldsymbol{r} \rho_{\rm tot}(\boldsymbol{r}) V(\boldsymbol{r})$. Thus we can modify $V(\boldsymbol{r})$, where $\rho_{\rm tot}(\boldsymbol{r})$ is negligibly small without affecting the total energy.
[29] J. P. Perdew, K. Burke, and M. Ernzerhof, Phys. Rev. Lett. **77**, 3865 (1996).
[30] J. P. Perdew, K. Burke, and M. Ernzerhof, Phys. Rev. Lett. **78**, 1396 (1997).
[31] N. Troullier and J. L. Martins, Phys. Rev. B **43**, 1993 (1991).
[32] L. Kleinman and D. M. Bylander, Phys. Rev. Lett. **48**, 1425 (1982).
[33] J. Yamauchi, M. Tsukada, S. Watanabe, and O. Sugino, Phys. Rev. B **54**, 5586 (1996); H. Kageshima and K. Shiraishi, *ibid.* **56**, 14985 (1997); O. Sugino and A. Oshiyama, Phys. Rev. Lett. **68**, 1858 (1992).

[34] O. Stern, Z. Elektrochem. Angew. Phys. Chem. **30**, 508 (1924).
[35] Note that we define the electron charge as positive to keep consistency with the convention of a PW-PP scheme.
[36] W. E. Pickett, Comput. Phys. Rep. **9**, 115 (1989).
[37] To accomplish this condition, we can choose appropriate η at any time.
[38] G. B. Bachelet, D. R. Hamann, and M. Schlüter, Phys. Rev. B **26**, 4199 (1982).